Sensors & Actuators: B. Chemical 271 (2018) 44–53

Contents lists available at ScienceDirect

Sensors and Actuators B: Chemical

journal homepage: www.elsevier.com/locate/snb

Enhanced sensing properties of SnO_2 nanofibers with a novel structure by carbonization

Ning Xie, Lanlan Guo, Fang Chen, Xueying Kou, Chong Wang, Jian Ma, Yanfeng Sun*, Fangmeng Liu, Xishuang Liang, Yuan Gao, Xu Yan, Geyu Lu*

State Key Laboratory on Integrated Optoelectronics, Key Laboratory of Gas Sensors, Jilin Province, College of Electronic Science and Engineering, Jilin University, 2699 Qianjin Street, Changchun 130012, People's Republic of China

ARTICLE INFO

Keywords:
Carbonization
Electrospinning
Porous structure
Gas sensor

ABSTRACT

Carbonization followed by calcination in air has been developed to synthesize porous SnO_2 based nanofibers. The precursor nanofibers were synthesized through electrospinning. The optimal synthesized condition was investigated according to the gas sensing properties of pure SnO_2 nanofibers through adjusting the heating rate in air. Gas sensors based on 1% Pd doped SnO_2 nanofibers under this optimal synthesized condition were fabricated, and the gas sensing properties was systematically investigated. The experimental results indicate that all the carbonized nanofibers have a porous microstructure. For the pure SnO_2 nanofibers, carbonized nanofibers also have a hollow structure. At the optimal synthesized condition, the sensor based on the carbonized SnO_2 nanofibers Exhibits 2.6 times higher response (20.4) than pristine pure SnO_2 nanofibers (7.7) toward 100 ppm ethanol. However, the selectivity is almost unchanged. For the Pd doped SnO_2 nanofibers, the gas response is improved from 10 to 24.6 to 100 ppm toluene at optimum operation temperature under the carbonization process. The sensors also exhibit a low detecting limit (1.6–500 ppb toluene) and a short response time (~3 s). The evolution process and the formation mechanism were also discussed.

1. Introduction

The development of industry and drastic improvement of life quality have increased the demands for harmful gas monitoring and detection [1]. Online detection of gas species is prerequisite for both the quality control in industrial production [2] and air-quality monitoring in city [3]. Furthermore, selective detection of trace specific volatile organic gas in exhale for non-invasive medical diagnostics is pushing the development of high sensitive gas sensors for detection of sub-ppm concentration of specific analytes (e.g. toluene) [4]. Until now, gas chromatography [5], mass chromatography [6] and ion mobility spectrometry [7] have been widely used to detect a number of VOCs with extreme sensitivity. However, these sensing techniques can't be used extensively due to the large size of the equipment, complexity of operation and high cost.

On the other hand, metal oxide based gas sensors make it possible for the realization of portable real-time gas sensors due to their small sizes, simple operation, low cost and easy fabrication. Since the report about gas-sensing properties of mental oxides in 1962 [8], extensive researches have been devoted to the optimization of mental oxide gas sensors with respect to their gas response, response speed, selectivity and economic efficiency (low costs and operation temperature) [9]. According to the physical and chemical properties of metal oxide materials, three basic factors (receptor function, transducer function and utility factor) were proposed by Prof. Yamazoe et al. to account for gas sensing properties [10]. According to the theory, porous structure seems to be a promising strategy for the enhancement of gas sensing performance because such structure facilitates more target gas to diffuse into or out of the sensing body, which can increase the gas response and reduce the response and recovery times [11–15]. Conventional sol-gel technology is often used to synthesize porous metal oxides which are used as gas sensing materials [16–19]. However, such method often needs strict reaction condition, and the repeatability is not very good. In addition, the as-prepared materials will lose some porosity after calcination at high temperature [20]. Crystalline mesoporous metal oxides have also been fabricated by using mesoporous silica as hard templates [21,22]. The shortcoming of this method is the necessity for the removal of silica template at alkaline environment.

Metal oxides fabricated through electrospinning not only possess the 1D nanostructures caused by the fabrication process, but also have the porous structure due to the elimination of polymer and the crystallization of the ceramic precursor. Both of them have been identified

* Corresponding authors.
E-mail addresses: syf@jlu.edu.cn (Y. Sun), lugy@jlu.edu.cn (G. Lu).

https://doi.org/10.1016/j.snb.2018.05.039
Received 12 January 2018; Received in revised form 6 May 2018; Accepted 9 May 2018
Available online 12 May 2018

as the most promising characteristics for the enhancement of gas sensing properties [23–27]. Various morphologies consisting of different pores and inconsecutive segments have been achieved through adjusting the key factors, such as flow-rate [28], volatile solvent [29], a phase-separation-inducing agent [30], the miscibility of polymer [23,31] and etc. Prof. Kim's group have done some excellent works about this aspect [32,33]. They successfully controlled both the size and distribution of spherical pores in electrospun WO_3 nanofibers through using polystyrene colloids with different diameters as the sacrificial templates, and enhanced gas sensing properties for H_2S detection was obtained [32]. Furthermore, they synthesized catalyst-loaded porous WO_3 nanofibers through using a novel catalyst functionalization method, which is based on protein-encapsulated metallic nanoparticles and their self-assembly on polystyrene colloid templates, and H_2S sensing performances was furtherly improved [33]. As for the SnO_2 nanofibers, stem-branch ZnO-SnO_2 nanofibers [34], SnO_2-ZnO core-shell nanofibers [35] and reduced grapheme oxide-loaded Au@SnO_2 nanofibers [36] were synthesized through electrospinning combined with vapor liquid solid method, atomic layer deposition and sol-gel method, and a great improvement of gas sensing properties to the target gas was observed. Size dependent sensing properties through changing the calcination temperature and duration [37] and loading effect of CuO using in-situ loading method [38] for SnO_2 nanofibers were also investigated. Especially, Kim et al. have reported a new synthetic approach for preparing catalysts loaded multidimensional nanostructures composed of 1D nanotubes and 0D hollow spheres through using carbonization process followed by calcination in air [39]. In their work, apoferritin was utilized to confine the grain size of catalysts and fulfill the even distribution of catalysts on SnO_2 nanostructure. Inspired by their ideas, we adopted different carbonization process and furtherly studied the effect of calcination process on gas sensing properties and morphology changes of the sensing materials through adjusting the heating rate in air. For Pd doped SnO_2 nanofiber, we just simply added the Pd salt into the precursor solution without using any extra organic material such as apoferritin.

Herein, we have designed a universal strategy to synthesize porous nanofibers through carbonization of the precursor nanofibers via electrospinning, followed by a simple calcination process at high temperature in air. Both pure and Pd doped SnO_2 nanofibers with and without carbonization method were prepared. The influence of the carbonization method to the morphology characteristics and gas-sensing properties were also investigated. As expected, the responses of the gas sensors based on both pure and Pd doped SnO_2 nanofibers show an obvious improvement after carbonization treatment. In addition, Pd doped SnO_2 nanofibers exhibited a novel structure due to the carbonization process. The possible formation and gas sensing mechanisms were also discussed in this paper.

2. Experimental procedures

2.1. Preparation of pristine pure SnO_2 nanofibers and Pd-doped SnO_2 nanofibers

All the chemicals used in this experiment are of analytical reagent grade without further treatment. Firstly, the SnO_2 nanofibers and Pd-doped SnO_2 nanofibers were prepared without carbonization. The pure and Pd-doped SnO_2 nanofibers were all synthesized by electrospinning, labeled as S1 and S2, respectively. Briefly, a certain amount of $PdCl_2$ (molar ratio was 0 and 1.0 mol% to SnO_2) and $SnCl_2{\cdot}2H_2O$ were dispersed in a mixture solution of 5 mL absolute ethanol and 5 mL DMF by magnetic stirring for 30 min at room temperature. Afterwards, 10 wt% of PVP was added into the mixed solution severally and continued stirring for 5 h at 50 °C to obtain a viscous precursor solution. After complete stirring, the solution was transferred into the syringe attached with a spinneret. The voltage and distance between the needle and the collector were 12.5 KV and 13 cm during the electrospinning process. The feeding rate of the solution was set as 0.3 mL/h by using a syringe pump. After electrospinning, the as-spun nanofibers were collected and calcined in air at 500 °C for 2 h with a heating rate of 2 °C/min to obtain the pristine pure and Pd doped SnO_2 nanofibers.

2.2. Preparation of porous pure SnO_2 and Pd-doped nanofibers with carbonization

In this process, the as-spun nanofibers mentioned above were used as the precursors. Before carbonization, the precursors were firstly heated in air at 230 °C for 30 min with a heating rate of 5 °C/min for stabilization. Then, the nanofibers were thermally heated up to 400 °C and maintained for 2 h with a heating rate of 2 °C/min in a tube furnace under N_2 atmosphere. Followed the carbonization process, the black nanofibers without Pd doping were subsequently heated to 500 °C with different heating rates (2 °C/min, 5 °C/min) for 2 h under air ambient, and the porous pure SnO_2 nanofibers were labeled as S3 and S4, respectively. Furthermore, the Pd-doped as-spun nanofibers were carbonized in a same way, and calcified in air with a heating rate of 2 °C/min. The as-obtained sample was denoted as S5.

2.3. Structural characterization

The x-ray diffraction (XRD) were observed by a Rigaku TTRIII X-ray diffractometer with Cu-Kα1 radiation (λ = 0.15406 nm) in the range of 20–80° (2θ) at room temperature. Field emission scanning electron microscopy (FESEM) images were collected using a JEOLJSM–7500 F microscope with an acceleration voltage of 15KV. The energy-dispersive X-ray spectroscopy (EDX) spots pattern scanning analysis was obtained by the TEM attachment. Transmission electron microscopic (TEM) and high-resolution transmission electron microscopic (HRTEM) images and selected area electron diffractive (SAED) patterns were obtained on a JEOLJEM-3010 transmission electron microscope with an acceleration voltage of 200KV. X-ray photoelectron spectroscopy (XPS) was performed on an ESCALABMKII X-ray photoelectron spectrometer.

2.4. Fabrication and measurement of gas sensors

The fabrication process of gas sensors with different SnO_2 samples is described as follows: the nanofibers were pressed on an alumina substrate (area = 1.0 mm × 1.5 mm, thickness = 0.2 mm) with two Au electrodes on its top surface and a micro-heater composed of ruthenium oxides on its bottom surface. The sensor temperatures are controlled by using the micro-heater and measured using an FLIR temperature sensor (T250, FLIR Systems Inc., USA). The sensors will be stabilized and the samples can have a good contact with the electrodes with the appropriate pressuring. The substrates were subsequently sintered at 450 °C (2 °C/min) for 2 h in air for the further stability of the sensors. The gas-sensing properties were measured at different temperature by changing the heater power. The concentration of gases was controlled by the adjusting the ratio between the gas and the air. The gas responses ($S = R_a/R_g$; R_a: resistance in air; R_g: resistance in gas) of different gases were measured by collecting the resistances upon exposure to air and target gases. The response and recovery time is defined as the time taken by the sensor to achieve 90% of the total resistance change when exposed to air and target gases, respectively [40,41].

3. Results and discussion

3.1. Structural and morphological characteristics

The XRD patterns of the as-synthesized samples (S1: pristine SnO_2, S2: pristine Pd-SnO_2, S3: carbonized SnO_2 with 2 °C/min, S4: carbonized SnO_2 with 5 °C/min and S5: carbonized Pd-SnO_2 with 2 °C/min) are shown in Fig. 1. All of the diffraction peaks are in good agreement with those of the SnO_2 standard card (No. 21–1250), and no other

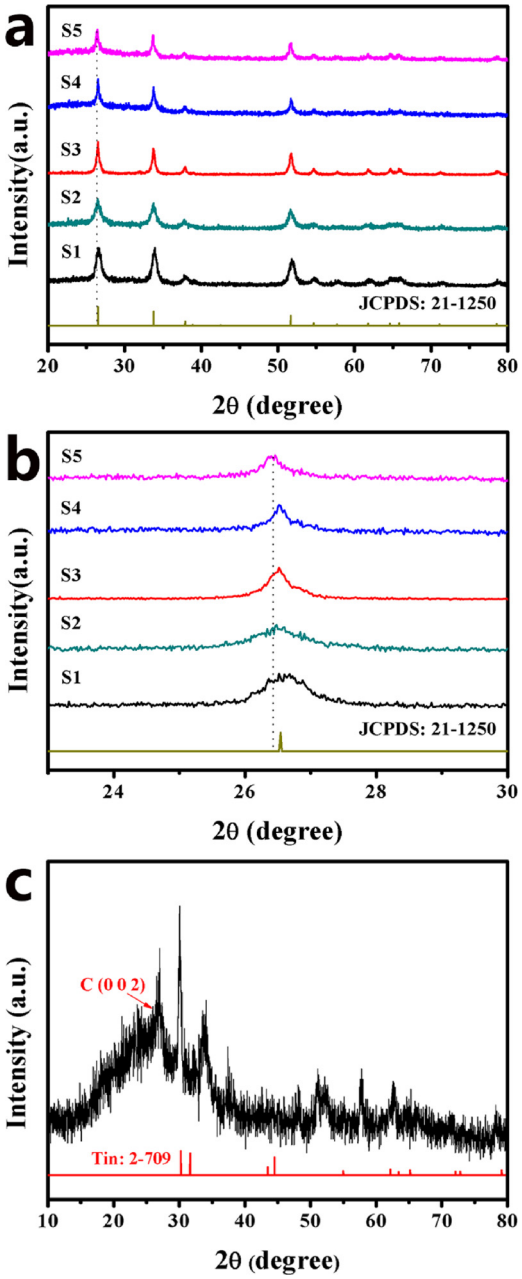

Fig 1. (a) XRD patterns of S1-S5 samples, (b) comparison of (110) peaks from XRD patterns and (c) XRD patterns of carbonized nanofibers without calcination in air.

diffraction peaks especially the peaks belonging to Pd or its oxides can be observed, confirming the phase purify of these nanofibers. The crystalline sizes of the as-synthesized samples were calculated to be about 14.67 nm, 12.04 nm, 22.73 nm, 25.85 nm and 18.63 nm according to the Debye-Scherrer formula [38]. It is obvious that Pd doping has decreased the crystals sizes, and the carbonization process has increased the crystal size. Compared with the S4 samples, the grain size of S3 samples is reduced with the heating rate changed from 5 °C/min to 2 °C/min, which could enhance the gas sensing properties [37]. Furthermore, the diffraction peaks have a little shift to the left with Pd doping as shown in Fig. 1b. This might be due to the larger radius of Pd^{2+} ions (0.086 nm) than that of Sn^{4+} (0.069 nm). Based on Bragg equation, the peaks should shift to left with Pd doping [42]. The results also indicate that Pd ions have entered the SnO_2 lattice successfully. None peaks shift is observed in the products due to the carbonization

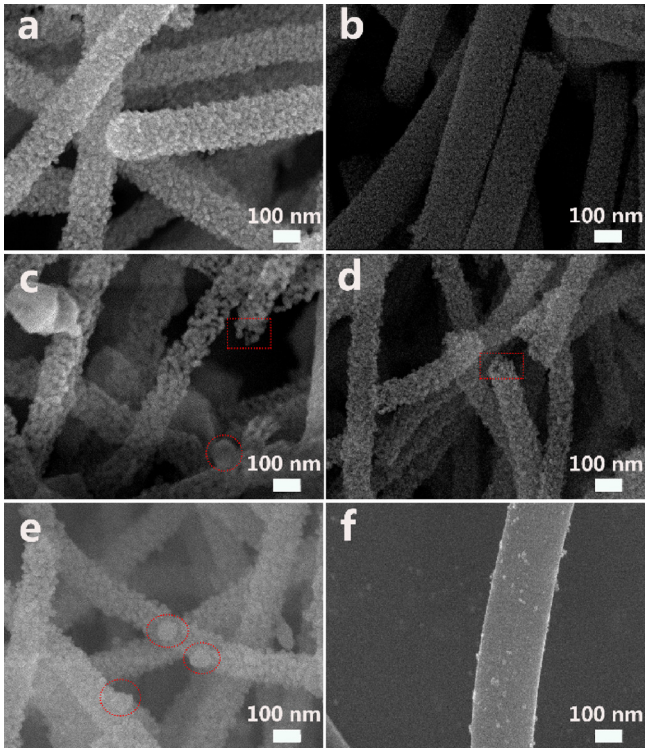

Fig. 2. FESEM images of (a) S1, (b) S2, (c) S3, (d) S4 and (e) S5 samples. (f) FESEM images of carbonized NFs without calcination in air.

process. The XRD patterns of the as-spun nanofibers after carbonization in N_2 were also collected (Fig. 1c). The peak appearing in the range of 20° to 30° is in agreement with the C (0 0 2) [43]. The diffraction peaks of tin metal are also found in the XRD patterns. The results indicate that the PVP was decomposed and carbonized, and Sn^{2+} was reduced to metal and embed in the nanofiber at the same time during the calcination in N_2.

The morphology was confirmed by SEM examination as shown in Fig. 2. Pure and Pd doped SnO_2 nanofibers without carbonization are displayed in Fig. 2a–b. It can be observed that the surface of the nanofibers with Pd doping (as shown in Fig. 2b) was obviously smoother than that of pure SnO_2 nanofibers (as shown in Fig. 2a). It is reasonable because of the decrease of crystal size caused by Pd doping, which is also in accordance with the XRD results. Fig. 2c–d show the morphology of pure carbonized nanofibers with different heating rate (2 °C/min and 5 °C/min) in air, and all the carbonized nanofibers possess a porous hollow structure. The hollow structure can be verified through the red rectangles marked in Fig. 2c and d. Moreover, the structure of the nanofibers became more porous through reducing the heating rate in air from 5 °C/min to 2 °C/min, and some big nanoparticles appeared on the surface of S3 samples (marked by red circle in Fig. 2c). Such porous structure is definitely beneficial for gas sensing enhancement [44,45]. The SEM image of carbonized Pd doped SnO_2 nanofibers (S5 sample) with the heating rate of 2 °C/min in air is shown in Fig. 2e (S5 sample). Due to the carbonization treatment, the surface of S5 samples becomes rougher compared with that of S2 sample (Fig. 2b). There are also some big nanoparticles appearing on the surface of S5 sample, which is similar with S3 sample calcified at the same heating rate of 2 °C/min in air. The morphology of the as-spun nanofiber after carbonization treatment is shown in Fig. 2f. The nanofibers exhibits smoother surface and larger diameter compared with the samples after calcination in air at high temperature. It indicates that the porous structure of S3-S5 samples might be due to the removal of the carbon materials at high temperature in air.

Further morphological and structural information of carbonized Pd

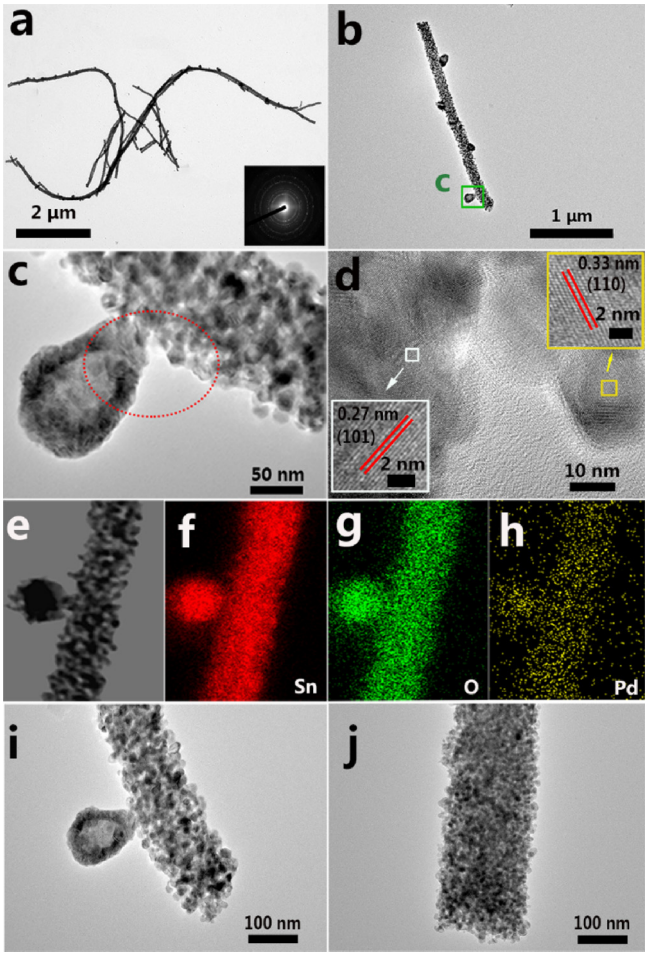

Fig. 3. (a)–(c) TEM image of S5 sample. The inset of (a) is the corresponding SAED pattern. (d) HRTEM images of the marked section in (c). (f)–(h) The corresponding elemental mapping images of (e). (i, j) TEM images of S5 and S2 samples in the same magnification respectively.

doped SnO_2 nanofibers (S5 sample) were provided by the TEM images as shown in Fig. 3. Fig. 3a shows the panoramic imagine of S5 sample, and the nanofiber structure can be confirmed. The insert of Fig. 3a shows the SAED pattern, demonstrating the complex features of these nanofibers [46,47]. More detailed structure can be seen from the enlarged TEM image in Fig. 3b. It can be observed that some big nanoparticles are almost periodically hanged on the surface of the nanofibers, which is in accordance with the SEM results. Fig. 3c is the TEM image corresponding to the green rectangle of Fig. 3b. It is clearly that only a small part of the big nanoparticle is connected with the nanofibers. The bright and dark spots on the nanofiber further verified the porous structure. The HRTEM images obtained from the marked circle in Fig. 3c are shown in Fig. 3d. The lattice spacing value from the nanofibers is about 0.33 nm, which is matched with the (110) planes of SnO_2. The other marked spacing value of the spheres is 0.27 nm, corresponding to (101) planes of SnO_2, which proves that the spheres on the nanofibers are also the SnO_2 particles. The EDX elemental mapping images (Fig. 3e–h) further confirm the composition of the product and the spatial distribution of Sn, Pd, and O in the nanofibers. As shown in Fig. 3h, Pd elements are detected in the whole region of the nanostructure, which indicates the uniform distributions of Pd element over the whole Pd doped SnO_2 porous nanofibers. Fig. 3i and j show the TEM images of carbonized and pristine Pd-doped SnO_2 nanofibers (S5 and S2 samples), respectively. Compared with S2 sample as shown in Fig. 3j, S5 sample (Fig. 3i) exhibited looser structure, and the particle size of S5 sample was obvious larger than that of S2 samples.

To further confirm the mechanism of the enhanced sensing performance, X-ray photoelectron spectroscopy (XPS) was used to investigate the electronic-states and surface chemical composition of elements for all synthesized nanofibers as shown in Fig. 4. Fig. 4a–e show the O 1s peaks of S1–S5 samples separately. The O 1s peaks are asymmetric and can be fitted into three different components. The binding energies located at about 530.4 eV (O_L), 531 eV (O_V) and 532 eV (O_C) correspond to lattice oxygen, oxygen vacancy and chemisorbed oxygen species, respectively [42,48]. The percentage of different oxygen components in different samples were also estimated by using the intensity of the relevant peaks in O 1 s XPS peaks, and the percentage and the center position were listed in Table 1. It is obvious that the content of O_C of dense Pd doped SnO_2 nanofibers (S2 sample) increases greatly compared with that of pristine SnO_2 nanofibers (S1 samples). It indicates that Pd doping is effective for the increase of Oc content. Carbonization treatment also has a great influence on the Oc content. After carbonization treatment, the Oc contents of S3 sample and S4 sample become larger compared with that of pristine SnO_2 nanofibers (S1 samples). Furthermore, the Oc content of S3 sample (27.7%) is higher than that of S4 sample (16.9%). This might be due to the different calcination speeds of S3 sample (2 °C/min) and S4 sample. It demonstrates that slower calcination process is beneficial for the increase of Oc content of the samples. Through using the slower calcination speed (2 °C/min), the Oc content of Pd doped nanofibers (S5 sample) exhibits the highest value (39.5%) among these samples. These results indicate that carbonization treatment and Pd doping are both beneficial for the enhancement of Oc content of the samples, and highest Oc content can be obtain through combing these two methods together. Fig. 4f shows the Sn 3d spectra of S5 samples. The peaks at binding energies of 495.3 eV and 486.85 eV are $3d_{3/2}$ and $3d_{5/2}$ peaks, respectively. This result demonstrates that Sn in the nanofibers all have a valence of +4. The Pd 3d peaks of S5 samples are presented in Fig. 4g. The peaks at binding energy 341.75 eV are attributed to Pd $3d_{3/2}$ and the 336.6 eV are for Pd $3d_{5/2}$, which all correspond to the values of PdO as shown in Fig. 4g [49].

3.2. Gas-sensing characteristics

The gas sensing properties of the as-synthesized nanofibers were investigated, and the influence of carbonization on the sensing properties was studied. The operating temperature is a significant parameter for gas sensors which mainly influence the response value and selectivity properties of the gas sensors. For this reason, the gas responses of the gas sensors based on pure nanofibers with and without carbonization treatment (S1, S3 and S4 samples) toward 100 ppm ethanol were measured at different working temperature as shown in Fig. 5a. The responses of all these sensors based on S1, S3 and S4 samples toward 100 ppm ethanol reach a maximum at the same working temperature (250 °C), which means that carbonization treatment will not change the optimal working temperature. After carbonization treatment followed by calcination in air at 5 °C/min, the response toward 100 ppm ethanol increases from 7.6 (S1 sample) to 14.5 (S4 sample). Through slowing the calcination speed (2 °C/min), the response of the gas sensors based on S3 sample is further increased and reaches to 20.4. The results indicate that carbonization treatment is helpful for the enhancement of gas response, and slower calcination process is also beneficial for the improvement of gas response.

The responses of the gas sensors based on pure nanofibers (S1, S3 and S4 samples) to 100 ppm various VOCs (ethanol, acetone, toluene, formaldehyde and methanol) are shown in Fig. 5b. It is obvious that all of the sensors show highest responses to the same concentration of ethanol. Towards all of the selected gases, the responses of the gas sensor based on S1 sample are the lowest. After carbonization treatment, the responses of the gas sensors to all of the VOC gases increase regardless of the gas species. Especially, the sensors based on S3 sample show the highest response compared with the other two sensors. The

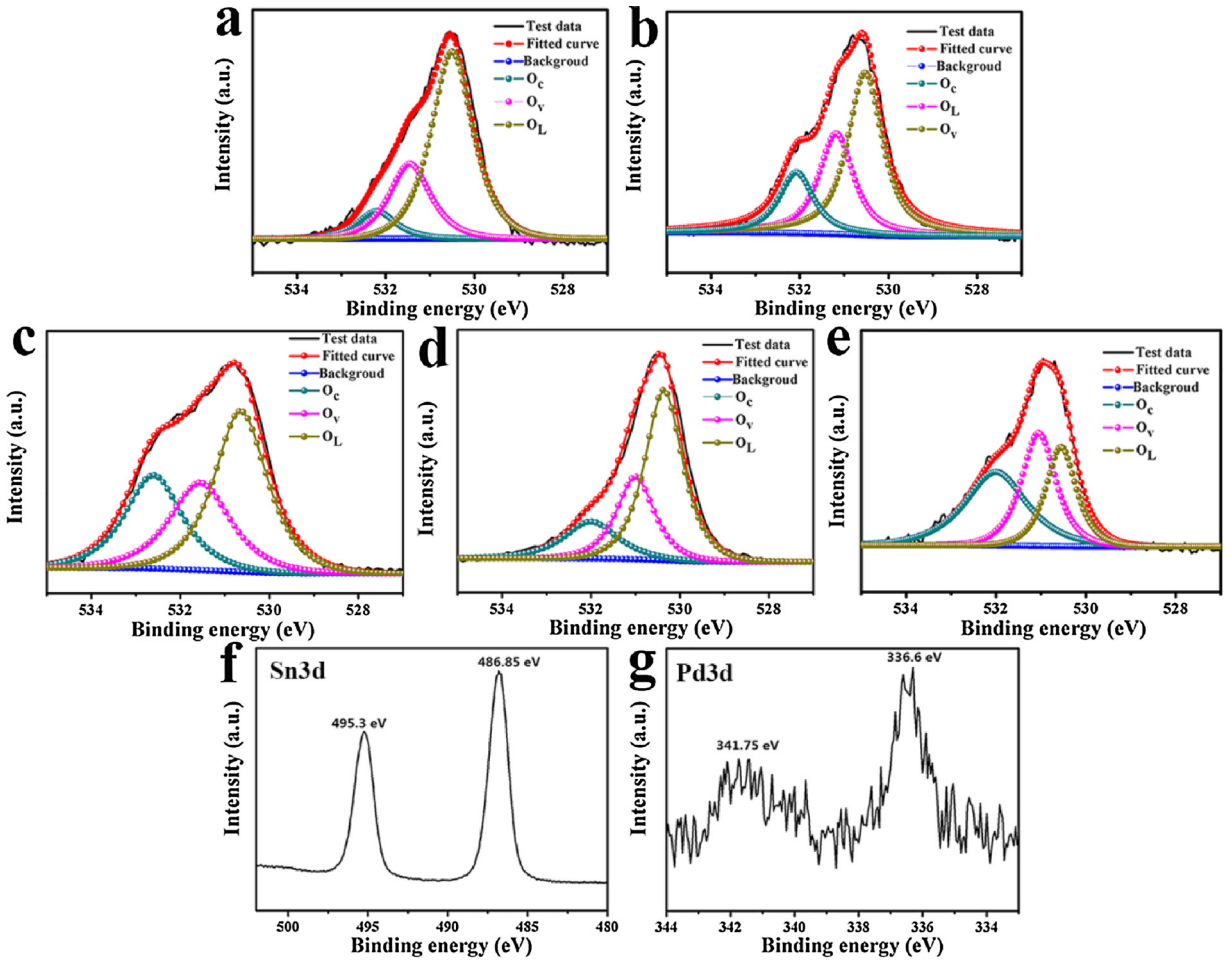

Fig. 4. XPS spectra of the obtained materials: (a)-(e) O 1s spectra of S1-S5 samples, respectively. (d) Sn 3d and (e) Pd 3d spectra of S5 sample.

Table 1
Fitting results of the O 1s XPS spectra of prepared nanofibers.

Samples	Oxygen species	Binding energy (eV)	Relative percentage (%)
Pristine SnO_2 (S1)	O_L (Sn-O)	530.5	64.9%
	O_V (vacancy)	531.45	26.3%
	O_C (chemisorbed)	532.2	8.8%
Pristine 1% Pd doped SnO_2 (S2)	O_L (Sn-O)	530.52	50%
	O_V (vacancy)	531.17	32%
	O_C (chemisorbed)	532.1	18%
Carbonized SnO_2 (2 °C/min) (S3)	O_L (Sn-O)	530.64	45.6%
	O_V (vacancy)	531.55	27.7%
	O_C (chemisorbed)	532.6	27.7%
Carbonized SnO_2 (5 °C/min) (S4)	O_L (Sn-O)	530.36	55.9%
	O_V (vacancy)	531	27.1%
	O_C (chemisorbed)	532	16.9%
Carbonized 1% Pd-SnO_2 (S5)	O_L (Sn-O)	530.55	26.3%
	O_V (vacancy)	531.05	34.2%
	O_C (chemisorbed)	532.0	39.5%

results indicate that carbonization treatment will generally increase the gas responses to all of the VOC gases, and the selectivity properties will not change much. Fig. 5c–e display the sensing transients of the gas sensors based on S1, S3 and S4 samples to 100 ppm ethanol at the working temperature of 250 °C. These results demonstrate that the sensors can restore to their original states after the removal of the ethanol gas. By the way, the response times can also be shortened from 7 s (S1) to 2 s (S3) and 3 s (S4) after the carbonization treatment. Even though the recovery times of the sensors become longer after the carbonization treatment, slower calcination process can significantly shorten the recovery time from 57S (S4 sample) to 29S (S3 sample).

Noble metal doping has significant effect on the gas sensing properties. As for the gas sensing properties based on Pd doped SnO_2 nanofibers (S2 and S5 samples), toluene was selected as the target gas and the gas sensing properties were investigated. Fig. 6a exhibits the response to 100 ppm toluene of the gas sensors based on pure SnO_2 nanofibers (S1 sample) and Pd doped SnO_2 nanofibers (S2 and S5 samples). Without Pd doping, the response of the sensor based on pure SnO_2 nanofiber is only about 3.0 at the optimal working temperature of 280 °C. After Pd doping (S2 sample), the response of the sensor based on Pd doped SnO_2 nanofibers becomes higher (from 3.1 to 10.2), and the optimal working temperature becomes lower (250 °C). Carbonization treatment (S5 samples) does not change the optimal working temperature (250 °C), but the response is significantly enhanced and reaches to 24.6 towards 100 ppm toluene. The selectivity of the gas sensors based on S1, S2 and S5 samples were also investigated as shown in Fig. 4b. It is obvious that Pd doping is effective for the selective detection of toluene. The carbonization effect for the Pd doped nanofibers is similar with the pure SnO_2 nanofibers. That is the carbonization treatment will generally increase the gas responses to all of the VOC gases, and the selectivity properties will not change much. Fig. 6c-e displays the sensing transients of the sensors based on S1, S2 and S5 samples to 100 ppm toluene at their optimum temperature. All of the sensors can response quickly upon exposure to toluene gas, and restore to their original states after the removal of the toluene gas. In addition, carbonization treatment can also shorten the recovery times from 75 s (S2 sample) to 35 s (S5 sample). Fig. 7a shows five reversible cycles of the response curves of the porous Pd doped SnO_2 nanofibers with carbonization treatment (S5 sample) to 100 ppm toluene, which confirms

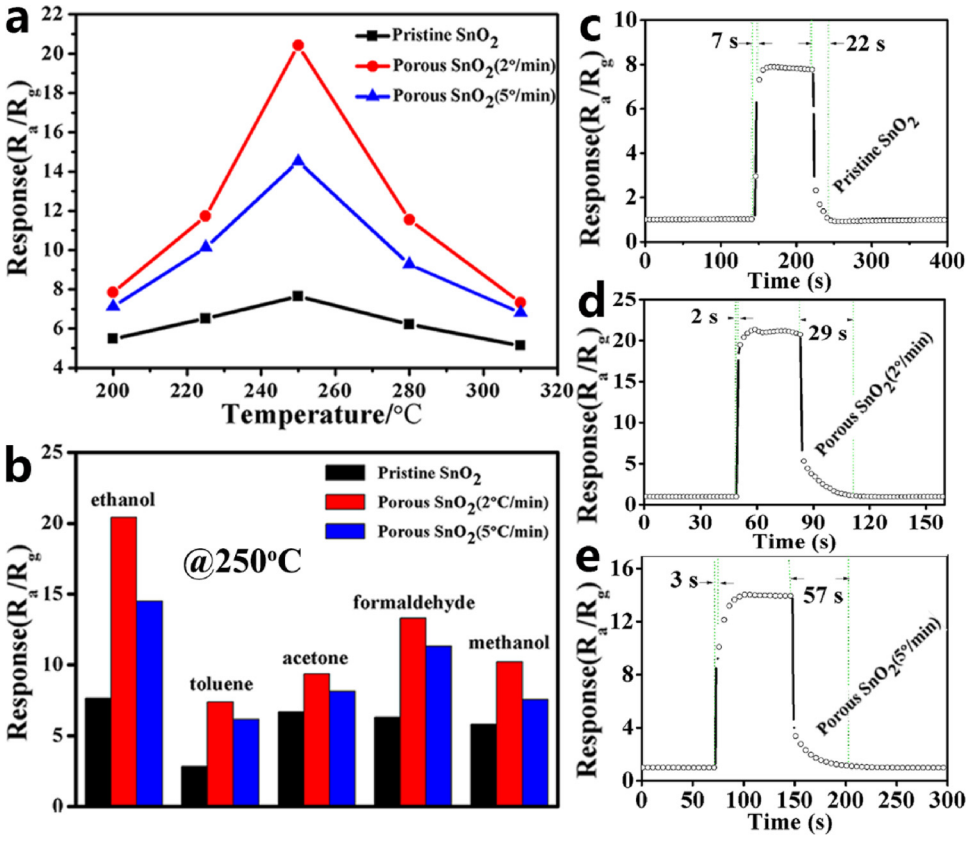

Fig. 5. (a) Response of the sensors based on S1, S3 and S4 samples to 100 ppm ethanol at different operating temperature, (b) response of the sensors based on S1, S3 and S4 samples to 100 ppm various test gases at 250 °C. (c)–(e) response-recovery characters of the sensors based on S1, S3 and S4 samples to 100 ppm ethanol at 250 °C respectively.

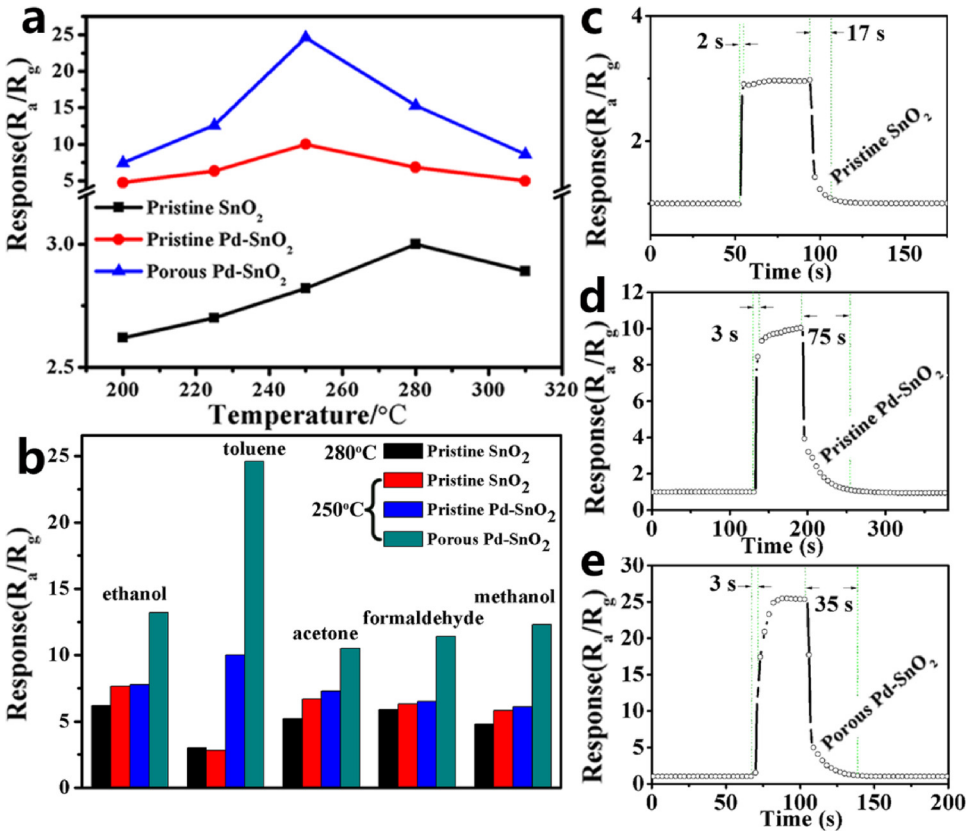

Fig. 6. (a) Response of the sensors based on S1, S2 and S5 samples to 100 ppm toluene at different operating temperature, (b) response of the sensors based on S1 at 250 °C and 280 °C, S2 and S5 samples at 250 °C to 100 ppm various test gases. (c)–(e) response-recovery characters of the sensors based on S1, S2 and S5 samples to 100 ppm toluene at their optimum working temperature respectively.

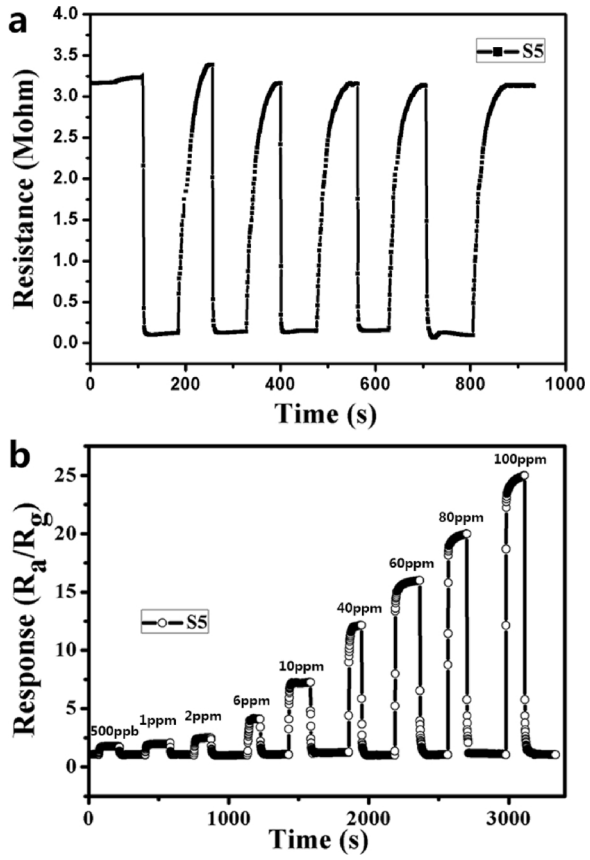

Fig. 7. (a) Five periods of response-recovery curves to 100 ppm toluene of the sensors based S5 sample, (b) dynamic response of the sensors based on S5 sample to different concentrations of toluene at 250 °C.

the reproducible and stable properties of the gas sensors. The response transients of the gas sensor based on porous Pd doped nanofiber (S5 sample) to different concentration of toluene gases is shown in Fig. 7b. It can be seen that shows a stepwise-increase with the toluene concentration from 500 ppb to 100 ppm. Furthermore, the sensor has a low detection limit and the response to 500 ppb toluene is about 1.6.

3.3. Formation mechanism

It is shown above that the morphology of nanofibers can be significantly influenced by carbonization treatment. To further investigate the formation mechanism, thermogravimetric Analysis (TGA) of the obtained precursor and carbonized nanofibers without calcination in air was performed as shown in Fig. 8. For the obtained precursor nanofiber,

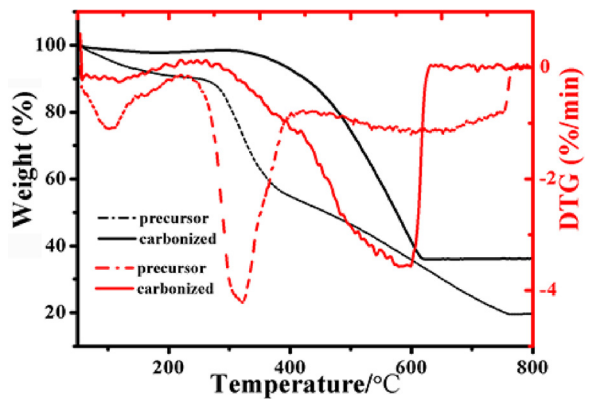

Fig. 8. TGA curves of as-spun nanofibers and carbonized nanofibers.

a sharp weight loss in the temperature range of 60–250 °C can be observed due to the evaporation of the trapped solvent. However, the weight loss at 100 °C is comparably lower for the carbonized nanofibers relative to that of the precursor nanofibers because of the evaporation of the solvent during the pre-oxidized process. Furthermore, two other weight losses are observed in the precursor. A weight loss occurred from 250 to 390 °C and reached the highest loss rate at 320 °C. This change indicates that the decomposition of PVP take place in this stage. Another slower weight loss can attribute to the further decomposition of PVP and crystallites can be observed in the temperature range of 390–750 °C [50]. For the carbonized nanofibers, only one obvious weight loss is observed in the temperature interval of 300–600 °C in the figure. The weight loss stopped at about 600 °C, suggesting the complete decomposition of carbon. The schematic formation process of the obtained nanofibers is shown in Fig. 9. As shown in Fig. 9a, the dense SnO_2 nanofibers were formed due to the shrinkage effect induced by thermal decomposition of PVP [51]. For the carbonized nanofibers, two processes are contained during calcination in air: decomposition of carbon and transformation of metal Sn to SnO_2. As shown in Fig. 8, the decomposition of carbon starts at about 300 °C, which is higher than the melting point of metal Sn (230 °C), indicating that the solid metal Sn will be transformed into liquid before the decomposition of the carbon. The weight loss continues to the end of the calcination, confirming that the carbon are gradually decomposed in the whole formation process of the nanofibers. At the same time, the Sn metal will transform into SnO_2. When the carbon are completely decomposed, the Sn metal is also transformed into SnO_2 material completely. Before the decomposition of carbon and after the transformation of Sn metal into liquid Sn, a part of Sn liquid will outflow from the inside of the carbonized nanofibers and cover on the surface. It is due to the lower density of liquid Sn than solid Sn. The volume expansion of Sn material makes it extruded by the carbon skeleton. The liquid Sn on the surface of nanofibers will transform to SnO_2 before the inner liquid Sn. Thus, the external SnO_2 could act as a template for the further formation of the inner SnO_2, and the hollow structure can be formed. Owing to the high decomposing temperature of carbon, the being formed SnO_2 will be separated by carbon throughout the calcination process in air. Therefor the porous structure of the nanofibers can be formed by the decomposition of carbon. As a result, porous SnO_2 nanofibers with a hollow structure can be fabricated as shown in Fig. 9b–c. The influence of the heating rate on the morphologies of porous SnO_2 nanofibers is also illustrated in Fig. 9. At a high heating rate (5 °C/min), not much Sn metal will transform into liquid Sn before the decomposition of carbon. Therefore, the effusive liquid Sn can only form a thin layer on the surface of the carbon material. When the heating rate in air is reduced to 2 °C/min, more liquid Sn will outflow from the nanofibers and coagulate into big balls due to the sufficient time between the melting of Sn metal and the decomposition of carbon. According, some big ball can be seen on the surface of the finally prepared nanofibers as shown in Fig. 9b and d. Nevertheless, porous Pd doped SnO_2 nanofibers with carbonization treatment does not exhibit a hollow structure. Such result might be due to the inhibition effect of Pd elements. The inner liquid Sn might be quickly transformed into SnO_2 with the decomposition of carbon at the help of Pd elements, and does not have enough time to move outwards. Therefore, a widely distribution of SnO_2 nanoparticles in the nanofibers are formed without forming the hollow structure as shown in Fig. 9d.

3.4. Gas sensing mechanism

For SnO_2 gas sensors, the most widely accepted sensing mechanism is based on space-charge model involving the charge transfer [52,53]. As a typical n-type semiconductor, the resistance of SnO_2-based sensors will increase due to the oxygen adsorption. When exposed to air, the oxygen adsorption will occur on the surface of the SnO_2 materials, and the extent of adsorption is up to the state of the interface, the specific surface area and the density of the active sites on the surface and so on.

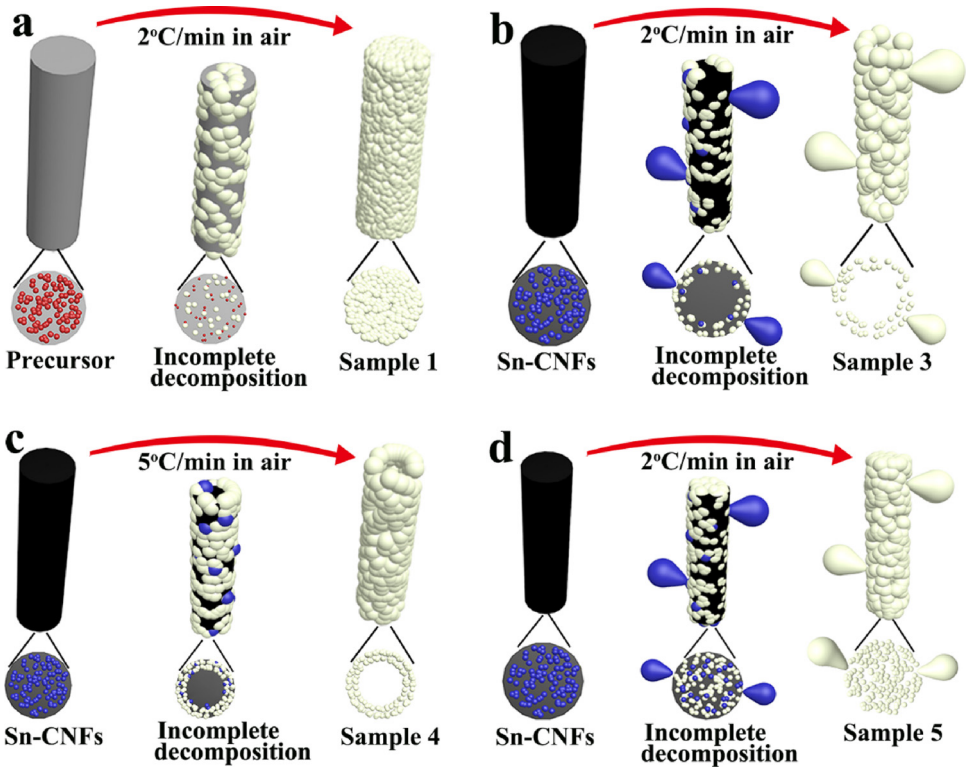

Fig. 9. Schematic diagram of the formation mechanism of (a) S1, (b) S3, (c) S4 and (d) S5 samples.

The adsorbed oxygen can capture the electrons from the conduction band of the SnO_2, and are ionized to oxygen ions such as $O_{2(ads)}^-$, $O^-_{(ads)}$ and $O^{2-}_{(ads)}$, decreasing the electron concentration and which is the main factor contributing to the increasing resistance [54]. When exposed to reducing gases such as toluene and ethanol, the gases will also be adsorbed and react with the oxygen ions adsorbed on the surface of the sensing material resulting in the release of the captured electrons [55]. And the electrons will go back to the conduction band, which leads to the reduction of the sensors resistance.

The enhanced gas sensing performance after carbonization treatment in this work can be attributed to the following aspects. As mentioned above, the removal of carbon species will lead to the formation of the porous structure (Fig. 2) and the increase of surface area (Fig. S1) for both pure and Pd doped SnO_2 nanofibers. Such porous structure can facilitate the diffusion of the target gases into the inner part of the sensing body with only slight consumption of the target gases, and the utility factor can be enhanced significantly. Therefore, the gas response is improved. Especially, some big particles will appear on the surface of the porous nanofibers when the heating rate in air is reduced from 5 °C/min to 2 °C/min. These big particles just hang on the surface of the nanofibers and have little contribution to the resistance of the nanofibers. It means that the gas response will not be obviously influenced by these big particles. The big particles might be caused by the more outflowing of the liquid Sn at slower heating rate, indicating that less Sn materials are left in the carbon skeleton before the decomposition of carbon. Therefore, more porous structure can be obtained at slower heating rate, which is beneficial for the enhancement of gas response. Besides the porous structure, the increase of the chemisorbed oxygen (Oc) after the carbonization treatment is the other reason for the enhancement of gas response to the target gases. For both pure and Pd doped SnO_2 nanofibers, the Oc contents are significant increased after the carbonization treatment verified by the XPS results. The Oc will react with the reduced gas directly and more electrons will return to the sensing materials, leading to the enhancement of gas response. The reason for the enhancement of the Oc contents after carbonization treatment might be redox reaction of carbon species during the formation of SnO_2 nanoparticles. Such reaction might lower the oxygen supply to the Sn metal during the formation of SnO_2 particles. Furthermore, a part of oxygen atoms of SnO_2 nanoparticles might be consumed due to the combustion of carbon species. Therefore, more oxygen defects can be formed which lead to more chemisorbed oxygen (Oc) compared with the traditional method. In conclusion, the carbonization treatment of the electrospun pure and Pd doped SnO_2 nanofibers is beneficial for the formation of porous structure and optimization of the surface state, which lead to the high gas response to the target gases.

4. Conclusion

In summary, novel porous SnO_2 nanofibers and Pd doped SnO_2 nanofibers were prepared by electrospinning to investigate the influence of the carbonization treatment on the gas sensing properties. The characterization results confirm that the carbonized nanofibers exhibit a porous structure. At lower heating rate in air, some big particles will appear on the surface of nanofibers, which leads to a more porous structure. The gas sensing investigations indicate that the carbonization treatment is an effective measure to improve the gas response for both pure SnO_2 and Pd doped SnO_2 nanofibers, and the responses to all gases have an obvious enhancement after carbonization treatment. Thus, the selectivity of the gas sensors is almost unchanged. The improvement might be ascribed to the formation of the porous structure, increase of surface area and more chemisorbed oxygen induced by the carbonization treatment.

Acknowledgements

This work was supported by National Nature Science Foundation of China (Nos. 61573164, 61520106003, 61327804). National High-Tech Research and Development Program of China (863 Program, No. 2014AA06A505).

Appendix A. Supplementary data

Supplementary data associated with this article can be found, in the online version, at https://doi.org/10.1016/j.snb.2018.05.039.

References

[1] G. Eranna, B.C. Joshi, D.P. Runthala, R.P. Gupta, Oxide materials for development of integrated gas sensors – a comprehensive review, Crit. Rev. Solid State Mater. Sci. 29 (2004) 111–188.

[2] S. Majumder, S. Hussain, R. Bhar, A.K. Pal, Liquid petroleum gas sensor based on SnO2/Pd composite films deposited on Si/SiO2 substrates, Vacuum 81 (2007) 985–996.

[3] J.S.G. Dos Santos-Alves, R.F. Patier, The environmental control of atmospheric pollution. The framework directive and its development. The new European approach, Sens. Actuators B: Chem. 59 (1999) 69–74.

[4] D. Poli, P. Carbognani, M. Corradi, M. Goldoni, O. Acampa, B. Balbi, L. Bianchi, M. Rusca, A. Mutti, Exhaled volatile organic compounds in patients with non-small cell lung cancer: cross sectional and nested short-term follow-up study, Respir. Res. 6 (2005).

[5] J.M. Sanchez, R.D. Sacks, GC analysis of human breath with a series-coupled column ensemble and a multibed sorption trap, Anal. Chem. 75 (2003) 2231–2236.

[6] R. Mukhopadhyay, Dont waste your breath, Anal. Chem. 76 (2004) 273A–276A.

[7] H. Lord, Y.F. Yu, A. Segal, J. Pawliszyn, Breath analysis and monitoring by membrane extraction with sorbent interface, Anal. Chem. 74 (2002) 5650–5657.

[8] A.K.T. Seiyama, K. Fujishi, M. Nagatani, A new detector for gaseous components using semiconductive thin films, Anal. Chem. 34 (1962) 1502–1503.

[9] M. Tiemann, Porous metal oxides as gas sensors, Chem. Eur. J. 13 (2007) 8376–8388.

[10] N. Yamazoe, K. Shimanoe, New perspectives of gas sensor technology, Sens. Actuators B: Chem. 138 (2009) 100–107.

[11] C.-L. Zhu, H.-L. Yu, Y. Zhang, T.-S. Wang, Q.-Y. Ouyang, L.-H. Qi, Y.-J. Chen, X.-Y. Xue, Fe2O3/TiO2 Tube-like nanostructures: synthesis, structural transformation and the enhanced sensing properties, ACS Appl. Mater. Interfaces 4 (2012) 665–671.

[12] X. Gao, C. Li, Z. Yin, Y. Chen, Synthesis and H2S sensing performance of MoO3/Fe2(MoO4)3 yolk/shell nanostructures, RSC Adv. 5 (2015) 37703–37709.

[13] K.-I. Choi, H.-J. Kim, Y.C. Kang, J.-H. Lee, Ultraselective and ultrasensitive detection of H2S in highly humid atmosphere using CuO-loaded SnO2 hollow spheres for real-time diagnosis of halitosis, Sens. Actuators B: Chem. 194 (2014) 371–376.

[14] Y.-J. Chen, X.-M. Gao, X.-P. Di, Q.-Y. Ouyang, P. Gao, L.-H. Qi, C.-Y. Li, C.-L. Zhu, Porous iron molybdate nanorods: in situ diffusion synthesis and low-temperature H2S gas sensing, ACS Appl. Mater. Interfaces 5 (2013) 3267–3274.

[15] X. Li, H. Zhang, C. Feng, Y. Sun, J. Ma, C. Wang, G. Lu, Novel cage-like alpha-Fe2O3/SnO2 composite nanofibers by electrospinning for rapid gas sensing properties, RSC Adv. 4 (2014) 27552–27555.

[16] N.S. Baik, G. Sakai, N. Miura, N. Yamazoe, Preparation of stabilized nanosized tin oxide particles by hydrothermal treatment, J. Am. Ceram. Soc. 83 (2000) 2983–2987.

[17] D.D. Vuong, G. Sakai, K. Shimanoe, N. Yamazoe, Preparation of grain size-controlled tin oxide sols by hydrothermal treatment for thin film sensor application, Sens. Actuators B: Chem. 103 (2004) 386–391.

[18] F. Lu, S. Chen, S. Peng, Ultrafine SnO2 prepared by supercritical fluid drying technique (SCFDT) for gas sensors, Catal. Today 30 (1996) 183–188.

[19] A. Jitianu, Y. Altindag, M. Zaharescu, M. Wark, New SnO2 nano-clusters obtained by sol-gel route, structural characterization and their gas sensing applications, J. Sol-Gel Sci. Technol. 26 (2003) 483–488.

[20] G.S. Devi, T. Hyodo, Y. Shimizu, M. Egashira, Synthesis of mesoporous TiO2-based powders and their gas-sensing properties, Sens. Actuators B: Chem. 87 (2002) 122–129.

[21] W. Yue, W. Zhou, Crystalline mesoporous metal oxide, Progr. Nat. Sci. 18 (2008) 1329–1338.

[22] K.K. Zhu, B. Yue, W.Z. Zhou, H.Y. He, Preparation of three-dimensional chromium oxide porous single crystals templated by SBA-15, Chem. Commun. (2003) 98–99.

[23] J.S. Lee, O.S. Kwon, S.J. Park, E.Y. Park, S.A. You, H. Yoon, J. Jang, Fabrication of ultrafine metal-oxide-decorated carbon nanofibers for DMMP sensor application, ACS Nano 5 (2011) 7992–8001.

[24] S.-H. Choi, I.-S. Hwang, J.-H. Lee, S.-G. Oh, I.-D. Kim, Microstructural control and selective C2H5OH sensing properties of Zn2SnO4 nanofibers prepared by electrospinning, Chem. Commun. 47 (2011) 9315–9317.

[25] L. Guo, X. Kou, M. Ding, C. Wang, L. Dong, H. Zhang, C. Feng, Y. Sun, Y. Gao, P. Sun, G. Lu, Reduced graphene oxide/alpha-Fe2O3 composite nanofibers for application in gas sensors, Sens. Actuators B: Chem. 244 (2017) 233–242.

[26] B. Ding, M. Wang, X. Wang, J. Yu, G. Sun, Electrospun nanomaterials for ultrasensitive sensors, Mater. Today 13 (2010) 16–27.

[27] D.-J. Yang, I. Kamienchick, D.Y. Youn, A. Rothschild, I.-D. Kim, Ultrasensitive and highly selective gas sensors based on electrospun SnO2 nanofibers modified by Pd loading, Adv. Funct. Mater. 20 (2010) 4258–4264.

[28] J. Shin, S.-J. Choi, I. Lee, D.-Y. Youn, C.O. Park, J.-H. Lee, H.L. Tuller, I.-D. Kim, Thin-wall assembled SnO2 fibers functionalized by catalytic Pt nanoparticles and their superior exhaled-breath-sensing properties for the diagnosis of diabetes, Adv. Funct. Mater. 23 (2013) 2357–2367.

[29] M. Bognitzki, W. Czado, T. Frese, A. Schaper, M. Hellwig, M. Steinhart, A. Greiner, J.H. Wendorff, Nanostructured fibers via electrospinning, Adv. Mater. 13 (2001) 70–72.

[30] Y. Hong, X. Chen, X. Jing, H. Fan, Z. Gu, X. Zhang, Fabrication and drug delivery of ultrathin mesoporous bioactive glass hollow fibers, Adv. Funct. Mater. 20 (2010) 1503–1510.

[31] Z. Zhang, X. Li, C. Wang, L. Wei, Y. Liu, C. Shao, ZnO hollow nanofibers: fabrication from facile single capillary electrospinning and applications in gas sensors, J. Phys. Chem. C 113 (2009) 19397–19403.

[32] S.-J. Choi, C. Choi, S.-J. Kim, H.-J. Cho, M. Hakim, S. Jeon, I.-D. Kim, Highly efficient electronic sensitization of non-oxidized graphene flakes on controlled pore-loaded WO3 nanofibers for selective detection of H2S molecules, Sci. Rep. 5 (2015) 8067.

[33] S.J. Choi, S.J. Kim, H.J. Cho, J.S. Jang, Y.M. Lin, H.L. Tuller, G.C. Rutledge, I.D. Kim, WO3 nanofiber-based biomarker detectors enabled by protein-encapsulated catalyst self-assembled on polystyrene colloid templates, Small 12 (2016) 911–920.

[34] S.-W. Choi, A. Katoch, G.-J. Sun, S.S. Kim, Synthesis and gas sensing performance of ZnO-SnO2 nanofiber-nanowire stem-branch heterostructure, Sens. Actuators B: Chem. 181 (2013) 787–794.

[35] A. Katoch, S.-W. Choi, G.-J. Sun, S.S. Kim, An approach to detecting a reducing gas by radial modulation of electron-depleted shells in core-shell nanofibers, J. Mater. Chem. A 1 (2013) 13588–13596.

[36] J.-H. Kim, A. Katoch, H.W. Kim, S.S. Kim, Realization of ppm-level CO detection with exceptionally high sensitivity using reduced graphene oxide-loaded SnO2 nanofibers with simultaneous Au functionalization, Chem. Commun. 52 (2016) 3832–3835.

[37] J.Y. Park, K. Asokan, S.-W. Choi, S.S. Kim, Growth kinetics of nanograins in SnO2 fibers and size dependent sensing properties, Sens. Actuators B: Chem. 152 (2011) 254–260.

[38] S.-W. Choi, J. Zhang, K. Akash, S.S. Kim, H2S sensing performance of electrospun CuO-loaded SnO2 nanofibers, Sens. Actuators B: Chem. 169 (2012) 54–60.

[39] J.S. Jang, S. Yu, S.J. Choi, S.J. Kim, W.T. Koo, I.D. Kim, Metal chelation assisted in situ migration and functionalization of catalysts on peapod-like hollow SnO2 toward a superior chemical sensor, Small 12 (2016) 5989–5997.

[40] C. Feng, X. Kou, B. Chen, G. Qian, Y. Sun, G. Lu, One-pot synthesis of In doped NiO nanofibers and their gas sensing properties, Sens. Actuators B: Chem. 253 (2017) 584–591.

[41] J.-H. Lee, Gas sensors using hierarchical and hollow oxide nanostructures: overview, Sens. Actuators B: Chem. 140 (2009) 319–336.

[42] X. Hu, Z. Zhu, C. Chen, T. Wen, X. Zhao, L. Xie, Highly sensitive H2S gas sensors based on Pd-doped CuO nanoflowers with low operating temperature, Sens. Actuators B: Chem. 253 (2017) 809–817.

[43] Q. Niu, J. Guo, B. Chen, J. Nie, X. Guo, G. Ma, Bimetal-organic frameworks/polymer core-shell nanofibers derived heteroatom-doped carbon materials as electrocatalysts for oxygen reduction reaction, Carbon 114 (2017) 250–260.

[44] M. Chen, Z. Wang, D. Han, F. Gu, G. Guo, Porous ZnO polygonal nanoflakes: synthesis, use in high-sensitivity NO2 gas sensor, and proposed mechanism of gas sensing, J. Phys. Chem. C 115 (2011) 12763–12773.

[45] C. Dong, Q. Li, G. Chen, X. Xiao, Y. Wang, Enhanced formaldehyde sensing performance of 3D hierarchical porous structure Pt-functionalized NiO via a facile solution combustion synthesis, Sens. Actuators B: Chem. 220 (2015) 171–179.

[46] D. Zhang, Y.E. Sun, C. Jiang, Y. Yao, D. Wang, Y. Zhang, Room-temperature highly sensitive CO gas sensor based on Ag-loaded zinc oxide/molybdenum disulfide ternary nanocomposite and its sensing properties, Sens. Actuators B Chem. 253 (2017) 1120–1128.

[47] R.C. Biswal, Pure and Pt-loaded gamma iron oxide as sensor for detection of sub ppm level of acetone, Sens. Actuators B: Chem. 157 (2011) 183–188.

[48] L. Gao, F. Ren, Z. Cheng, Y. Zhang, Q. Xiang, J. Xu, Porous corundum-type In2O3 nanoflowers: controllable synthesis, enhanced ethanol-sensing properties and response mechanism, Cryst. Eng. Comm. 17 (2015) 3268–3276.

[49] W.-T. Koo, S.-J. Choi, S.-J. Kim, J.-S. Jang, H.L. Tuller, I.-D. Kim, Heterogeneous sensitization of metal-organic framework driven metal@metal oxide complex catalysts on an oxide nanofiber scaffold toward superior gas sensors, J. Am. Chem. Soc. 138 (2016) 13431–13437.

[50] J. Wu, D. Zeng, X. Wang, L. Zeng, Q. Huang, G. Tang, C. Xie, Mechanistic insights into formation of SnO2 nanotubes: asynchronous decomposition of poly(vinylpyrrolidone) in electrospun fibers during calcining process, Langmuir 30 (2014) 11183–11189.

[51] B.R. Roo, S.T. Oh, H.J. Ahn, Camphene effect for morphological change of electrospun SnO2 nanofibres: from dense to fibre-in-hollow and to hollow nanostructures, Mater. Lett. 178 (2016) 288–291.

[52] J. Zhang, X. Liu, S. Wu, M. Xu, X. Guo, S. Wang, Au nanoparticle-decorated porous SnO2 hollow spheres: a new model for a chemical sensor, J. Mater. Chem. 20 (2010) 6453–6459.

[53] P. Mohanapriya, H. Segawa, K. Watanabe, K. Watanabe, S. Samitsu, T.S. Natarajan, N.V. Jaya, N. Ohashi, Enhanced ethanol-gas sensing performance of Ce-doped SnO2 hollow nanofibers prepared by electrospinning, Sens. Actuators B: Chem. 188 (2013) 872–878.

[54] F. Qu, J. Liu, Y. Wang, S. Wen, Y. Chen, X. Li, S. Ruan, Hierarchical Fe3O4@Co3O4 core-shell microspheres: preparation and acetone sensing properties, Sens. Actuators B: Chem. 199 (2014) 346–353.

[55] Y. Liu, G. Zhu, J. Chen, H. Xu, X. Shen, A. Yuan, Co3O4/ZnO nanocomposites for gas-sensing applications, Appl. Surf. Sci. 265 (2013) 379–384.

Ning Xie received the B. Eng. Degree in department of electronic sciences and technology in 2016. Now he is currently studying for degree of master at Jilin University. His work is the synthesis and characterization of the semiconducting functional materials and gas

sensors.

Lanlan Guo entered her MS course from department of Inorganic Chemistry, Jilin University, China, in 2014. Now, she is studying for her PhD degree, engaged in the synthesis and characterization of the semiconducting functional materials and gas sensors.

Fang Chen received her B. Eng. degree from the Electronics Science and Engineering department, Jilin University, China in 2017. Her work is the synthesis and characterization of the semiconducting functional materials and gas sensors.

Xueying Kou received the B. Eng. degree in department of electronic sciences and technology in 2015. She is currently studying for her M.E. Sci. degree in College of Electronic Science and Engineering, Jilin University, China. Now, she is engaged in the synthesis and characterization of the semiconducting functional materials and gas sensors.

Chong Wang received the B. Eng. degree in department of electronic sciences and technology, Jilin University, in 2013. At the same year, she entered her MS course in College of Electronic Science. Now, she is studying for her PhD degree, majored in the synthesis and characterization of the semiconducting functional materials and gas sensors.

Jian Ma received his MS in 2009 from Jilin University at the Electronics Science and Engineering department. Presently, he is working as Technical Assistant in Electronics Science and Engineering department. His current research interests are gas sensor, the design and fabrication of micro-hot plates.

Yanfeng Sun obtained his PhD from Jilin University of China in 2007. Presently, he is working as associate professor in Electronics Science and Engineering department of Jilin University. His current research interests are nanoscience and gas sensors.

Fangmeng Liu received his B.S. degree in 2009 from College of Chemistry, Liaocheng University and M.S. degree in 2012 from Northeast Forestry University in China. Currently he is studying for his Ph.D. degree in College of Electronic Science and Engineering, Jilin University, China.

Xishuang Liang received the B.Eng. degree in Department of Electronic Science and Technology in 2004. He received his Doctor's degree in College of Electronic Science and Engineering at Jilin University in 2009. Now he is an associate professor of Jilin University, China. His current research is solid electrolyte gas sensor.

Yuan Gao received her PhD degree from Department of Analytical Chemistry at Jilin University in 2012. Now she is a lecturer in Jilin University, China. Her current research is focus on the preparation and application of graphene oxide and semiconductor oxide, especial in gas sensor and biosensor.

Xu Yan received his M.S degree in 2013 from Nanjing Agricultural University. He joined the group of Prof. Xingguang Su at Jilin University and received his Ph.D. degree in June 2017. Since then, he did postdoctoral work with Prof. Geyu Lu. Currently, his research interests mainly focus on the development of the functional nanomaterials for chem/bio sensors.

Geyu Lu received the BS degree in electronic sciences in 1985 and the MS degree in 1988 from Jilin University in China and the Dr Eng degree in 1998 from Kyushu University in Japan. Now he is a professor of Jilin University, China. Now, he is interested in the development of functional materials and chemical sensors.